$Li_2Si_2O_5$ Nano-brush Coated Carbon Cloth as a Potential Solution for Wastewater Treatment

Bo Sun[a], Wenge Chen [a,*], Hui Zhang[a], Ahmed Elmarakbi[b], Yong-Qing Fu [b,*]

[a] School of Materials Science and Engineering, Xi'an University of Technology, Xi'an, Shaanxi, 710048, P.R. China

[b] Faculty of Engineering and Environment, Northumbria University, Newcastle upon Tyne, NE1 8ST, UK.

*Corresponding authors: Prof. Wenge Chen; Prof. Richard Yongqing Fu.

E-mail: wgchen001@263.net (W.G. Chen), richard.fu@northumbria.ac.uk (Y.Q. Fu)

Abstract

$Li_2Si_2O_5$ nano-brush coated carbon cloth was synthesized using a hydrothermal method with lithium hydroxide and tetraethyl orthosilicate as the resource chemicals. Its adsorption capabilities for Mn^{2+}, Cu^{2+} and Ni^{2+} ions were demonstrated for wastewater treatments, and their corresponding maximum adsorption capacities were 325.60, 312.12 and 270.15 mg/g at 298 K, respectively. Brush-like and highly uniformly $Li_2Si_2O_5$ nanorods with an average diameter of ~60 nm were uniformly synthesized onto the carbon cloth. Adsorption experiments showed that the adsorption behaviors for selected heavy metal ions followed both a pseudo-second-order model and a Langmuir isothermal model, indicating that the adsorption process was a monolayer and chemical adsorption one. The key adsorption mechanisms were identified as surface complexation between heavy metal ions and hydroxyl groups and ion-exchanges between heavy metal ions and lithium ions. These brush-like nanorods

have advantages of effective adsorption of heavy metal ions in wastewater due to their widely exposed active sites and effective ion diffusion and transport.

Keywords: Lithium disilicate; Carbon cloth; Heavy metal adsorption; Nanostructure

1. Introduction

With the rapid progress of world-wide industrialization and urbanization, a large amount of wastewater containing heavy metal ions are constantly discharged into natural environment, causing great threats to human beings, animals and environments [1-3]. Among these heavy metal ions, Ni can directly lead to pulmonary fibrosis, skin allergy and respiratory cancer [4]. Cu and Mn do not directly cause severe harm to human body, but they will potentially damage the liver, kidney and nervous system when they are accumulated in body for a long time [5, 6]. Currently various methods, including electrocoagulation [7], adsorption [8], anodic oxidation [9], biodegradation [10] and photocatalysis [11], have been proposed to remove heavy metal ions from water resources. Among them, adsorption, a method to remove pollutants directly from wastewater, has received significant attention because of its low cost, easy operation, high efficiency and low power consumption. In recent years, various adsorption materials have been developed, such as activated carbon [12], zeolite [13], chitosan [14] and metal organic framework [15]. They are usually dispersed into the water in the forms of powders, particulates or microfibers. However, they tend to agglomerate easily in the application process, which affects the adsorption performance. In addition, they are very difficult to separate after adsorption, which also results in so-called "secondary pollution" [16,17]. Up to now, little attention has been paid to develop free-standing and highly effective adsorbents for facile usage and separation.

Compared with other adsorption materials, silicate, one of the basic components of minerals with harmless to the environment and low cost, has excellent chemical stability and active adsorption performance due to its rich oxygen-containing functional groups on the surface [18,19]. Valenzuela et al. [20] previously synthesized nanostructured calcium silicates by adjusting the Ca/Si molar ratio, and used them as

an adsorbent to remove Cu^{2+} and Cd^{2+} ions from water, with adsorption capabilities of 25.83 mg/g and 16.21 mg/g, respectively. Bai et al. [21] prepared mesoporous manganese silicates with high oxygen containing functional groups, and reported their good selective adsorption performance for methylene blue, with the maximum adsorption capacity of 217 mg/g.

Among all these silicates, $Li_2Si_2O_5$ has a unique layered structure composed of $[SiO_4]$ tetrahedron frameworks with the mobile Li^+ ions resided among layers, and it contains rich oxygen-containing functional groups, which could be explored as ideal candidates of adsorbents for wastewater treatment [22,23]. In our previous work [24], lithium silicate was used as the adsorption material for heavy metal ions for the first time. We prepared lithium silicate with controllable structures by adjusting the Li/Si molar ratio of the precursors, and achieved the maximum adsorption capacity of Mn^{2+} and Cu^{2+} ions of 232.43 mg/g and 287 mg/g, respectively. However, we found that there are many problems remained such as low adsorption capacity, easy agglomeration of powders, and difficulties for separation and recycling.

The structure of the material greatly affects the adsorption performance. Zheng et al. [25] loaded CuO onto the surface of a carbon fiber paper, which greatly dispersed CuO and formed a 3D paper-structure, showing an excellent catalytic activity. If $Li_2Si_2O_5$ with its hierarchical nanostructures (such as nanorods or nano-brushes) can be directly synthesized onto a substrate, the adsorption sites on its surface can be fully exposed and the surface energy is increased, thus promoting the efficient adsorption of heavy metal ions. At the same time, the introduction of substrate materials can also solve the problem that those powder adsorbed materials are difficult to be separated after adsorption [26,27]. As another cheap and light source, carbon cloth has a unique porous structure, with its mechanical softness and strength as well as good chemical stability, all of which are suitable for being used as the supporting substrate for growth of micro- and nanostructures [28,29].

In this paper, we synthesized brush-like $Li_2Si_2O_5$ nanorods on carbon cloth using an one-step hydrothermal method for heavy metal ions adsorption in wastewater treatment. Lithium disilicate nanorods were uniformly loaded onto the surface of

carbon cloth to form a brush-like structure. Nanorods with a large aspect ratio show a large surface energy, and can easily adsorb heavy metal ions. At the same time, these brush structures prevent the agglomeration of lithium disilicates, thus exposing more active adsorption sites and leaving more spaces to maximize the adsorption performance of heavy metal ions in wastewater treatment. As a novel adsorption material, the brush-like $Li_2Si_2O_5$ nanorods coated carbon cloth showed an excellent adsorption efficiency for heavy metal ions in wastewater and easy separation of ions afterwards. For the demonstration of effective adsorptions of heavy metal ions using the prepared materials, in this study, we selected three elements (i.e., Mn^{2+}, Cu^{2+} and Ni^{2+}) as examples, and tested in the industry wastewater samples.

2. Experimental

2.1 Preparation of $Li_2Si_2O_5$ coated carbon cloth

Porous $Li_2Si_2O_5$ on carbon cloth was synthesized using a hydrothermal synthesis method as illustrated in Fig. 1. The carbon cloth was treated with a dilute nitric acid solution (2 mol/L) for removing its surface impurities and oxides, followed by an ethanol solution cleaning process, before being used as the substrate for growing $Li_2Si_2O_5$ nanostructures. Firstly, 0.672 g of $LiOH·H_2O$ (0.016 mol) was dissolved in 70 mL of water and stirred for 30 min to obtain a transparent solution. Then 3.334 g of tetraethyl orthosilicate (0.016 mol) was added dropwise into the above solution within 10 min. The Li/Si molar ratio in the solution was maintained as 1:1. This was followed by a continuous stirring for 30 min to obtain a uniform mixed solution. Finally, the above mixed solution was transferred into a polytetrafluoroethylene covered stainless steel autoclave liner (with a filling ratio of 80%), and a carbon cloth with a size 2cm×2cm was placed inside. This autoclave was kept at 180℃ for 6 hrs, and then naturally cooled down to room temperature. After this, the hydrothermal product was washed with distilled water and ethanol for several times, and then dried at 60℃ for 24 hrs. The prepared sample was nano-brush $Li_2Si_2O_5$ (lithium disilicate) coated carbon cloth, which is denoted as LDCC.

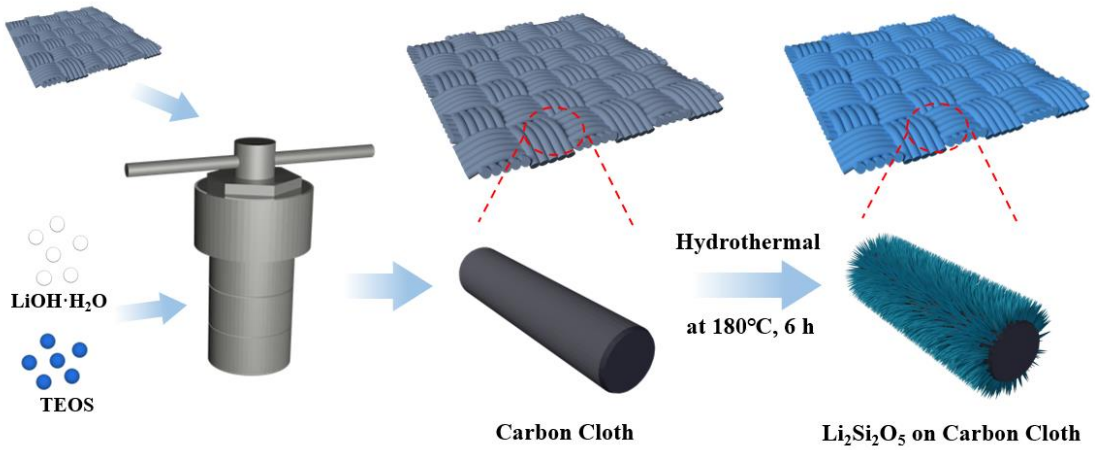

Fig. 1. Schematic illustrations of the fabrication processes of LDCC.

2.2 Material characterizations.

Surface morphology and microstructure of $Li_2Si_2O_5$ coated carbon cloth were observed using a scanning electron microscope (SEM, ZEISS Sigma 300), attached with an energy dispersive X-ray spectroscope (EDX, Oxford INCA) for chemical element analysis. Crystalline structures of the synthesized materials were studied using an X-ray diffractor (XRD, Bruker D8 ADVANCE) with Cu kα radiation. Chemical elements and their binding information were characterized using an X-ray photoelectron spectroscope (XPS, Thermo ESCALAB 250XI). Specific surface area, pore size and volume of products were measured by the Brunauer-Emmet-Teller (BET) method using N_2 adsorption-desorption isotherms (ASAP 2460, MICROMETER). The inner structures and their interactions were detected using a Fourier Transform Infrared spectrometer (FTIR, Nicolet iS 10). A Raman spectroscope (Horiba Scientific LabRAM HR Evolution) was also used and excited using a laser beam with a wavelength of 532 nm. The contents of metal ions in the solution were determined using an inductively coupled plasma based optical emission spectrometer (ICP-OES, PerkinElmer 8300). Zeta potentials were measured using a zeta potential analyzer (Malvern Zetasizer Nano ZS90).

2.3 Adsorption experiments

Adsorption performance of the LDCC for the heavy metal ions was evaluated using heavy metal ion solutions at different contact times, initial concentrations, mixed concentrations, and initial pH values. The carbon cloth samples with a $Li_2Si_2O_5$

loading rate of ~0.04 g/cm^2 were cut into a size of 1 cm × 1 cm, and directly used as the adsorbents. Solutions of $MnSO_4 \cdot H_2O$, $CuSO_4 \cdot 5H_2O$ and $NiSO_4 \cdot 6H_2O$ were prepared and used as the heavy metal ion solutions. Initially at the same concentration of 100 mg/L, the changes of LDCC's adsorption capacity as a function of contact duration were evaluated under a continuous stirring at 298 K for 24 hrs. The concentrations of individual type of heavy metal ions were then changed from 50 to 300 mg/L at different temperatures (e.g., 298 K, 308 K and 318 K), and the adsorption capacities of LDCC at different initial concentrations of heavy metals were evaluated. The initial pH value of the solution was adjusted to 2, 3, 4, 5 and 6 with different concentrations of diluted HCl solutions, and the effect of the initial pH value on the adsorption performance of LDCC at their initial concentration of 150 mg/L was evaluated. Mixtures of three types of heavy metal ion solutions with their concentrations of ions of 50 to 250 mg/L were prepared, and the effect of their concentration after adsorption using LDCC was measured under a continuous stirring at 298 K, to analyze the selective adsorption behavior of multiple heavy metal ions. In addition, the influences of coexistence of anions (Cl^-, NO_3^-, CO_3^{2-}, PO_4^{3-}) and cations (Na^+, K^+, Mg^{2+}, Al^{3+}) on the capability of LDCC to adsorb heavy metal ions were studied. The initial concentrations of anion, cation and heavy metal ions were fixed at 150 mg/L. To evaluate the practical application of LDCC, it as adsorbent was add directly to 100 mL wastewater obtained from a chemical milling factory under a continuous stirring at 298 K for 6 hrs. The regeneration process was also performed in an EDTA-2Na solution. The LDCC after adsorption was added to the solution and stirred for 24 h at room temperature, and then the adsorbent was collected by centrifugation and reapplied in the next adsorption process.

The adsorption capacity and removal efficiency (η) of LDCC was calculated using the following equation:

$$q = (C_0 - C_t) \times V/W \quad (1)$$

$$\eta = (C_0 - C_t)/C_0 \times 100\% \quad (2)$$

where q (mg/g) is the adsorption capacity at a given time t. C_0 and C_t (mg/L) are the heavy metals' initial concentration and the concentration at a time t (mg/L),

respectively. V (L) is the volume of the heavy metal ions solutions, and W (g) is the mass of the $Li_2Si_2O_5$ on carbon cloth.

3. Results and discussion

3.1 Characterization of $Li_2Si_2O_5$ on carbon cloth

Fig. 2 shows morphologies and nanostructures of $Li_2Si_2O_5$ grown on the carbon cloth using the hydrothermal method. The commercial carbon cloth shows woven carbon fibers with a diameter of about 10 μm (see Fig. 2(a)). After the hydrothermal treatment at 180°C, the surface of the carbon cloth was fully covered by white powders (see Fig. 2 (b1)) of $Li_2Si_2O_5$, and the $Li_2Si_2O_5$ obtained using the hydrothermal method is uniformly distributed on the carbon cloth (Fig. 2(b2)). Moreover, the prepared carbon cloth supported $Li_2Si_2O_5$ composite shows a good flexibility (see Fig. 2(c)). Fig. 2(d) shows the processes of LDCC after adsorption of Mn^{2+} ions and simple separation. The white LDCC sample was immersed into the Mn^{2+} ions solution and continuously stirred. After a period of time, the color of the sample was changed, indicating the apparent adsorption effect. The composite after absorption can be easily separated from the carbon cloth substrate, as can be clearly revealed from Fig. 2d.

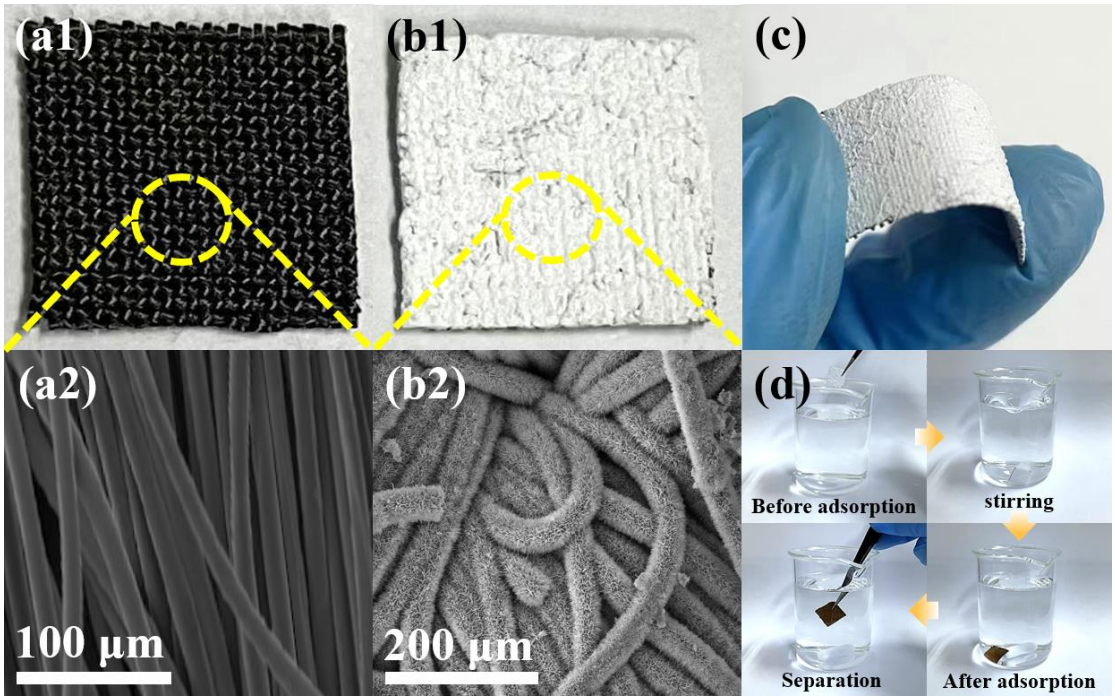

Fig. 2. (a1) and (a2) Macro-/microscale morphology of $Li_2Si_2O_5$ nanorods grown on carbon cloth. (b1) and (b2) Carbon cloth before loading. © Demonstration of flexibility of carbon cloth after loading. (d) Adsorption and separation phenomena of LDCC for the adsorption of Mn^{2+} ions.

Fig. 3 shows microstructures of carbon cloth supported $Li_2Si_2O_5$ composites. In Fig. 3(a), the $Li_2Si_2O_5$ with shapes of nanobrushes are assembled and grown on the carbon fibers. Higher magnification SEM images (Fig. 3(b) and (c)) show that these nanobrushes are composed of nanorods with an average diameter of 60 nm ± 200 nm and an average length of ~10 μm. Due to the woven structures of carbon fibers in the carbon cloth, these nanorods are also closely contacted with each other. Not only are these nanostructures stable, but also they are easily adsorb substances such as contaminants. In addition, these nanobrushes have many edges and sharp places, with large surface energy [30]. Therefore, this unique brush-like structure composed of nanorods can provide more active sites and spaces for capturing heavy metal ions. Large volumes of porous structures of these nanobrushes can be clearly observed as shown in the yellow frame in Fig. 3(c), which enables fast transport of heavy metal ions and also maximizes the adsorption capacity of the material. Fig. 3(d) shows EDX analysis results of the LDCC, which show that Si and O elements are evenly distributed throughout the nanorods. Au elements were also observed from the EDX spectrum, which is because of gold coating of samples before SEM observation. Li elements were not clearly identified because the beryllium window in the EDX absorbs X-ray of light elements such as Li [31]. The existence of Li element was proven in the following XRD and XPS results. Figs. 3(e-f) show the TEM images of the nanorods of $Li_2Si_2O_5$ and its corresponding selective area electron diffraction (SAED) image. The results reveal that each nanorod has single crystal characteristics, corresponding to the orthorhombic structure of $Li_2Si_2O_5$ [32]. The formation of these single crystals is because under both high temperature and high pressure, lithium and silicon sources formed dissolved products in the hydrothermal environment and reached a supersaturation. During the subsequent process, the solubility was reduced and precipitate was formed and grown into single crystals. Similar crystal growth mechanisms have been reported in our previous work [33, 34]. In addition, these single

crystal structures were found to be anisotropic, which is advantageous for the efficient diffusion of ions and exposure of more adsorption sites, thus improving the adsorption performance of the material [35].

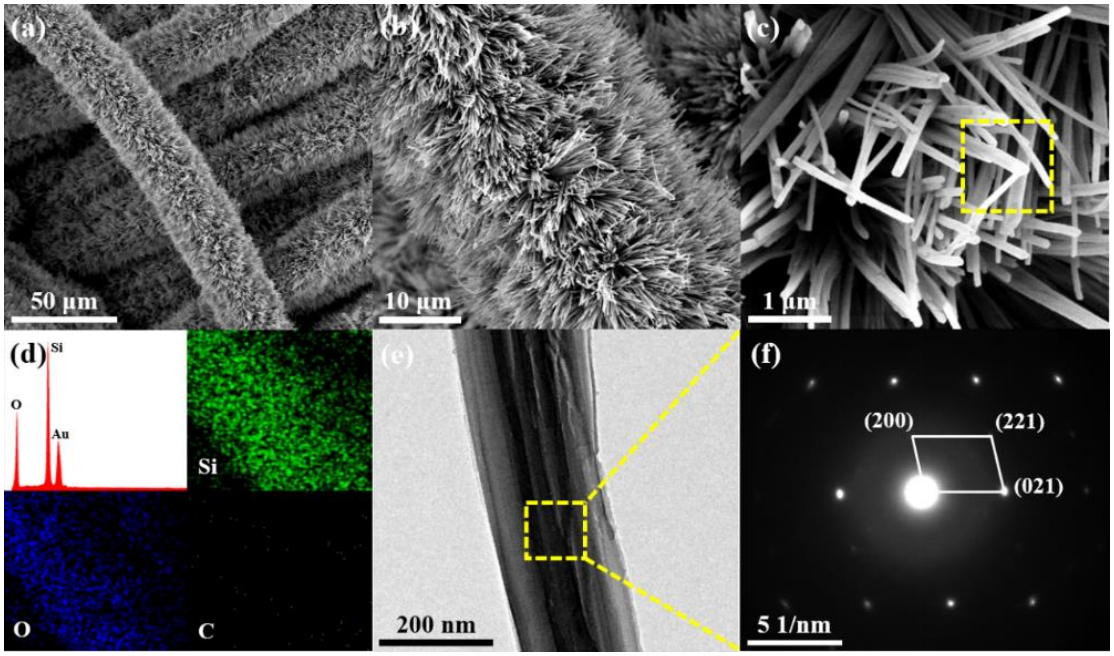

Fig. 3. (a-c) SEM images of LDCC. (d) EDX mapping image of Fig. (b). (e-f) TEM and SAED images of a single $Li_2Si_2O_5$ nanorod.

XRD spectrum of the LDCC is shown in Fig. 4(a). The diffraction peak at the 2θ angle of 25.6° is corresponding to the (002) crystal plane of carbon. Another diffraction peak (100) of the carbon cloth is identified at 43.5° [36]. The left diffraction peaks at the 2θ angles of 11.9°, 12.8°, 20.1°, 21.2°, 21.8°, 29.8°, 34.1° and 35.5° are related to the planes of (110), (020), (200), (210), (021), (221), (150), and (002) of $Li_2Si_2O_5$, respectively (JCPDS card no. 33-0816) [32, 35]. No other peaks were found from the XRD spectrum.

Fig. 4(b) shows the XPS survey spectrum of LDCC. It can be seen that there are no other elements except Li, Si, O and C in the LDCC. Figs. 4(c) and (d) show the N_2 adsorption-desorption isotherms and obtained pore size distribution of the LDCC. The sample shows the typical type IV isotherms with the H3 type hysteresis loop [37]. The isotherms have not leveled off at pressures close to the saturation vapor pressure and there are not parallel and horizontal branches, which indicates that lithium disilicate has a mesoporous structure. The porosity distribution was calculated by the N_2-Density

Functional Theory model (DFT), which showed two peaks centered at around 1.88 nm and 3.30 nm. The pore diameters of 1.88 nm and 3.30 nm were derived from the pores of lithium disilicates, and the pores generated by stacked nanorods, respectively. The Brunauer-Emmett-Teller (BET) specific surface area of LDCC was up to 9.27 m^2/g with the total pore volume of 0.059 cm^3/g.

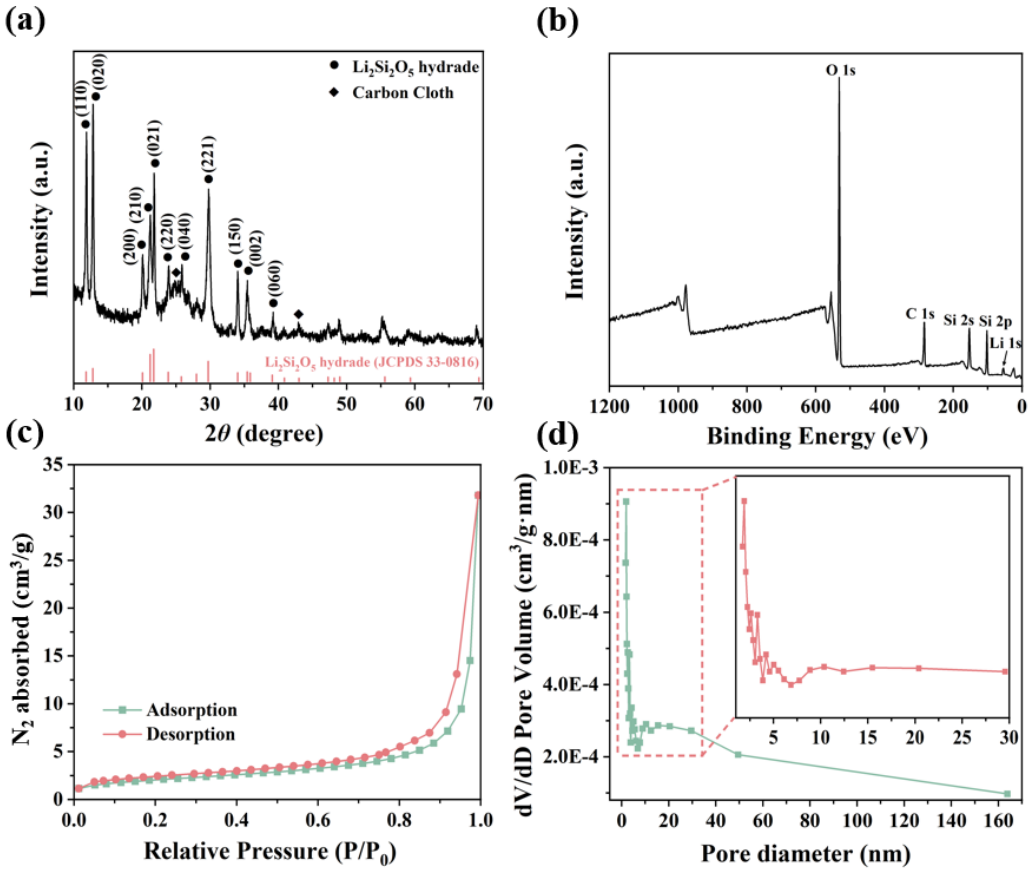

Fig. 4. (a) XRD patterns of the LDCC. (b) Survey XPS spectra of the LDCC. (c) N_2 adsorption-desorption isotherms of the LDCC. (d) Pore diameter distribution curve of the LDCC.

3.2 Adsorption performance of LDCC

Fig. 5(a) shows the obtained relationship between the adsorption capacity of the LDCC for heavy metal ions and the adsorption time. The values of q_t and q_e (mg/g) are the adsorption capacities of the LDCC at time t and an equilibrium time, respectively. C_e is the equilibrium concentration (mg/L). It can be seen that the adsorption curves obviously show two stages, i.e., the initial deceleration adsorption stage and the later equilibrium stage. The adsorption of heavy metal ions by the LDCC is quite rapid in the initial stage, which is mainly because there are numerous active sites and oxygen-containing functional groups on surfaces of LDCCs, which promotes the adsorption

effect. With the increase of contact time, the adsorption sites are gradually occupied by the adsorbates, thus the active areas are decreased. Simultaneously the adsorption rate is gradually decreased, finally reaching an equilibrium adsorption capacity [39].

Results also show that the adsorption rate of Mn^{2+} ions by the LDCC is the highest, followed by those of Cu^{2+} and Ni^{2+} ions. The main reason is because the ionic radius of Mn^{2+} ions is much larger than those of Cu^{2+} and Ni^{2+} ions, whereas the solubility product of Cu^{2+} ions is much smaller than that of Ni^{2+} ions [40]. The equilibrium adsorption capacities of LDCC for solutions with Mn^{2+}, Cu^{2+} and Ni^{2+} ions with a given ion concentration of 100 mg/L are 249.95, 249.93 and 249.87 mg/g, respectively.

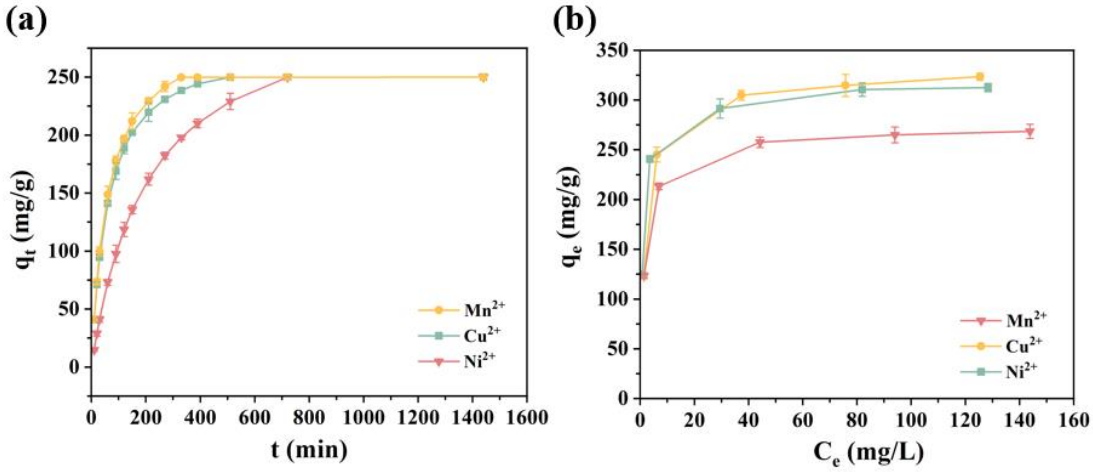

Fig. 5. (a) Effects of contact time on adsorption capacities of Mn^{2+}, Cu^{2+} and Ni^{2+} ions using LDCC. (b) Effects of initial concentration on adsorption capacities of Mn^{2+}, Cu^{2+} and Ni^{2+} ions using LDCC.

Fig. 5(b) shows the obtained results of LDCC's adsorption capacities for three types of heavy metal ions with different concentrations at different temperatures (i.e., 298 K, 308 K and 318 K). It can be seen that when the initial concentration of ions is low, the adsorption is enhanced rapidly, because at this stage, the adsorption sites have not been fully occupied. Results also show that with the increase of concentration of ions, the adsorption tends to become slower and gradually reaches its equilibrium adsorption capacity. The maximum adsorption capacity can be expressed by the adsorption capacity at the equilibrium condition. The obtained maximum adsorption capacities of LDCC for Mn^{2+}, Cu^{2+} and Ni^{2+} ions are 325.60, 312.12 and 270.15 mg/g at 298 K, respectively. The adsorption capacities of Mn^{2+}, Cu^{2+} and Ni^{2+} ions by the

LDCC are increased with the increases of their initial concentrations, which is mainly attributed to the increased driving forces of adsorption [41]. It was also found that the adsorption capacities of LDCC for these three heavy metal ions showed an upward trend between 288 K and 308 K, indicating that the process of heavy metal ions adsorbed onto LDCC has shown an endothermic nature. All the above results show that the lithium disilicate plays a major role in the adsorption of heavy metal ions in wastewater.

Fig. 6 summarizes the reported adsorption properties of many commonly used adsorption materials reported in literature, i.e., data from references of [42-52], as well as the data of nanobrush like LDCC in this study. The value of q_m is the maximum adsorption capacity of the LDCC (mg/g). Clearly, the LDCC prepared in this study has shown one of the best adsorption performances for heavy metal ions, compared with many of other reported materials in literature as seen in Fig. 6.

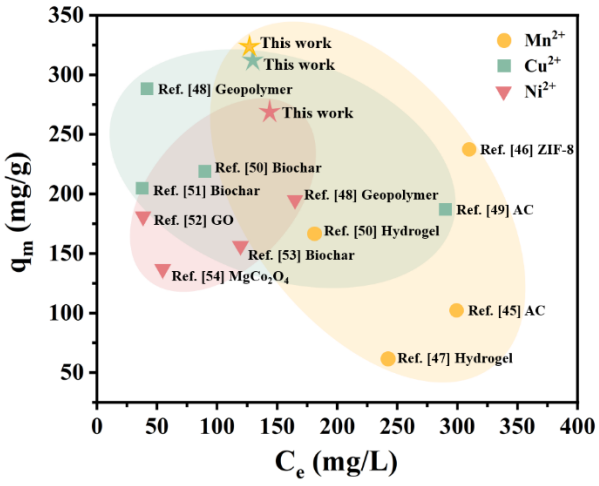

Fig. 6. Comparisons of adsorption properties among the reported adsorption materials and that of LDCC in this study (in which yellow, green and red areas represent Mn^{2+}, Cu^{2+} and Ni^{2+} ions, respectively).

The initial pH value of the aqueous solution is one of the important factors that significantly affect the adsorption behavior of the adsorbent. This is because there are strong adsorption competitions for the adsorption positions between hydrogen ions and heavy metal ions, and heavy metal ions could be hydrolyzed and precipitated in the alkaline solution. Therefore, we have further investigated the adsorption of the heavy metal ions at various pH values from 2 to 6 with an initial ion concentration of 150

mg/L. Fig. 7(a) shows the changes in the adsorption performance of LDCC for heavy metal ions at different pH values. It can be seen that the adsorption quantities of Mn^{2+}, Cu^{2+} and Ni^{2+} ions by the LDCC are increased with the increase of pH value of the system. At a lower pH value, there is a strong competition between H^+ ions and heavy metal ions occupied the same adsorption position on surface groups of the LDCC, thus resulting in a lower adsorption capacity of the LDCC [53]. With the increase of pH value, the competition between H^+ ions and adsorption sites are significantly reduced, and the interactions between heavy metal ions and adsorption sites are increased, so the adsorption capacity of the LDCC is gradually increased. In addition, the states of the functional groups are also altered by the proton concentrations at different pH values [54]. The higher the H^+ concentration, the easier the protonation of OH^- occur in an acidic condition, which may hinder the complexation of OH^- with heavy metal ions [55]. These two effects weaken the interactions between LDCC and heavy metal ions, thus decreasing the adsorption capacity of LDCC.

The surface charge of adsorbent may also be changed due to the changes of pH values of solutions. The changes of LDCC's surface charges promote the electrostatic attractions or repulsions between LDCC and heavy metal ions, thus resulting in the changes of adsorption capacities of the materials for heavy metal ions. Fig. 7(b) shows the effects of different initial pH values on the zeta potentials of LDCC. It can be seen that the zeta potential is lower than 0 mV for the LDCC with a lower pH range (e.g., below 6), but then it decreases with the increase of the pH value, indicating that there is a negative potential on the surface of LDCC. The zeta potentials at the pH values of the solutions from 2.0 to 6.0 are between -1.72 mV and -23.31 mV. At a lower pH value, there are abundant hydrogen ions, which compete with heavy metals for adsorption sites, and they will be preferentially exchanged with Li^+ ions rather than with heavy metal ions.

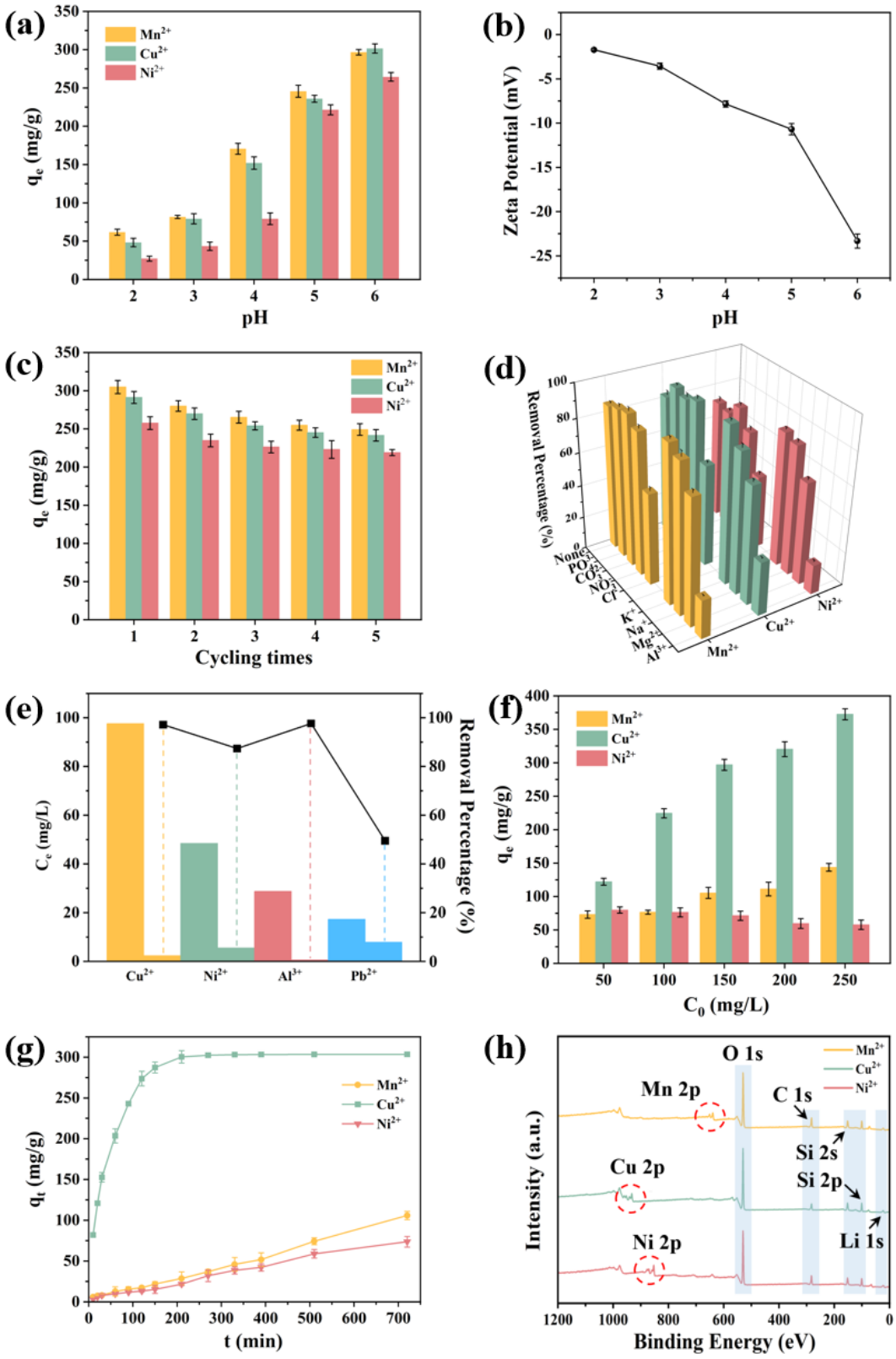

Fig. 7. (a) Effect of initial solution pH values on the adsorption of heavy metal ions. (b) Zeta potential of LDCC. (c) The cycling performance of LDCC for adsorbing heavy metal ions. (d) Effect of co-existing anions and cations on Mn^{2+}, Cu^{2+}, Ni^{2+} ions removed by LDCC. (e) Capacity and removal percentage of heavy metal ions in real wastewater before and after

adsorption. (f) Adsorption properties of LDCC for mixed ions with different initial concentrations. (g) Effect of contact time on adsorption capacity of the LDCC toward mixed ions. (h) XPS spectra of LDCC after Mn^{2+}, Cu^{2+} and Ni^{2+} adsorption.

To further assess the possibility of LDCC as an adsorption material for practical applications, cycling performance tests were conducted using the heavy metal ion solution with an initial concentration of 150 mg/L. The obtained results are shown in the Fig. 7(c). After five cycles, the adsorption capacities of LDCC for Mn^{2+}, Cu^{2+} and Ni^{2+} are decreased by 18.26%, 17.02% and 14.94% respectively. The main reasons for such decreases of LDCC's adsorption capacities are the destruction of the material structures, the occupied active functional groups and non-renewable active centers on the surface, and minor ion-exchanges [54, 55].

A small amount of lithium ions are normally produced due to ion-exchange in the solution after heavy metal ions are adsorbed by the composite. This can be solved by adding TEOS and NaOH into the solution, and our results show that white lithium disilicate precipitation was clearly produced in the solution. The reaction can be described using Eq. (3) [32]. Therefore, this process can be applied to facilitate the recovery and reuse of lithium ions during the practical applications.

$$2Li^+ + 2SiO_2 \cdot H_2O + 2OH^- = Li_2Si_2O_5 \cdot 2H_2O + H_2O \quad (3)$$

There are inevitably many anions and cations in practical wastewater, which will affect the migration of target heavy metal ions in environmental media. The commonly reported ions in wastewater include cations such as Na^+, K^+, Mg^{2+}, Al^{3+}, and anions such as Cl^-, NO_3^-, CO_3^{2-}, PO_4^{3-} [56]. In this study, we have further investigated their influences. Fig. 7(d) shows the influences of the above inorganic ions with a fixed concentration of 150 mg/L on the adsorption capabilities of Mn^{2+}, Cu^{2+} and Ni^{2+} ions by LDCC. Obviously, monovalent and divalent cations such as Na^+, K^+, Mg^{2+}, show little influences on the adsorption process. However, trivalent Al^{3+} show a strong inhibition effect, which significantly reduced the adsorption rates of Mn^{2+}, Cu^{2+} and Ni^{2+} on LDCC from 81.27%, 77.72% and 68.69% to 23.33%, 32.59% and 17.94%, respectively. This is because Al^{3+} ions have a higher valence state and a lower ionic radius than those of the other ions, and it also has a high affinity to LDCC [57]. These

cause the LDCC to preferentially adsorb Al^{3+}, as shown in Fig. S1. Among the anions studied, the adsorption rates of Mn^{2+}, Cu^{2+} and Ni^{2+} by LDCC in the presence of PO_4^{3-} were increased by 7.52%, 15.03% and 1.29%, respectively, compared with those without PO_4^{3-}. The reason is attributed to that the PO_4^{3-} reacted with Mn^{2+}, Cu^{2+} and Ni^{2+} adsorbed on the surface of LDCC and became a multi-component complex, thus becoming newly formed active centers for enhancing the adsorption [58]. Similarly, CO_3^{2-} also show the improved removal ability of three heavy metal ions. In contrast, Cl^- ions of the monovalent anion show an inhibitory effect on the adsorption of Mn^{2+}, Cu^{2+} and Ni^{2+} ions by LDCC. The reason is attributed to that Cl^- was strongly bonded to the non-ionized Si-OH or the $SiOMe^+$ group formed on the LDCC surface [59].

In order to verify the feasibility of the prepared composite for practical applications, we have directly used the synthesized composite as the adsorbent to the wastewater, which was obtained directly from a chemical milling factory. The obtained mixture was continuously stirred for 6 hrs during the process. The types and concentrations of heavy metal ions contained in the wastewater before and after removal are shown in the Fig. 7(e). It can be seen that the composite has shown excellent adsorption performance for Cu^{2+}, Ni^{2+} and Al^{3+} ions in the wastewater, and the removal percentage reaches 97.61%, 88.72% and 98.05%, respectively. The reason for the better adsorption performance of the Al^{3+} ions is that aluminum ions have higher valence than the other heavy metal ions, which makes them have higher affinity in the solution. In addition, it was found that the composite showed good adsorption properties for Pb^{2+} ions. The above results demonstrate that the prepared composite can be used in actual wastewater treatment.

When these mixed ions are coexisted in a mixture, they will compete for adsorption sites of the adsorbent, which would be interested to study. Here as a demonstration, we still use Cu^{2+}, Mn^{2+} and Ni^{2+} three ions for this study. Fig. 7(f) shows the adsorption effects for mixing these three heavy metal ions at different initial concentrations. It can be found that the LDCC has the best adsorption capacity for Cu^{2+} ions, followed by Mn^{2+} ions. As the initial concentration of mixed ions is increased, the adsorption capacity of Cu^{2+} ions are also increased, and the adsorption

capacity of the mixed ions is equivalent to that of single Cu^{2+} ions only. The adsorption capacity of Mn^{2+} ions is also increased with the increase of its initial concentration in the mixture, but the adsorption capacity in this mixture is decreased significantly compared with that of solution with only Mn^{2+} ions. The adsorption capacity of Ni^{2+} ions in this ion mixture is also decreased with the increase of its initial concentration. A reasonable explanation for these results is that the ionic radius of Cu^{2+} (0.077 nm) is larger than those of Mn^{2+} (0.067 nm) and Ni^{2+} (0.069 nm), and Cu^{2+} has a greater affinity for hydroxyl in the surface of LDCC [60]. These are mainly attributed to the differences in their chemical characteristics. As we know, Cu has a higher electronegativity (1.9) than those of Mn (1.55) and Ni (1.8) [61]. In addition, Cu ($Cu(OH)_2$:19.6) has a higher value of pK_{sp} (i.e., the negative log of solubility product constant) than both of those Mn ($Mn(OH)_2$:12.7) and Ni ($Ni(OH)_2$:14.7). These factors result in that Cu^{2+} ions are favorably adsorbed through surface complexation of LDCC or sorption reactions, compared with those of Mn^{2+} and Ni^{2+} ions. These results demonstrate that the adsorption behaviors of LDCC for Mn^{2+}, Cu^{2+} and Ni^{2+} ions are attributed to the following factors: (1) greater hydrolysis constant, (2) larger atomic weight, (3) larger ionic radius, and (4) higher solubility of the product, all of which provide Cu with improved efficacy for LDCC surface complexation or sorption reactions.

Fig. 7(g) shows the relationship between the adsorption amounts and adsorption time of LDCC when the initial concentration of mixed ions is 150 mg/L. It can be seen that for the adsorbed Cu^{2+} ions, the adsorption curve shows two stages, i.e., the initial deceleration adsorption stage and a later equilibrium stage, as already explained before. The adsorption of Cu^{2+} ions by the LDCC is increased rapidly in the initial contact stage, which is mainly because there are a large number of hydroxyl and numerous adsorption sites on the surface of LDCC, and Cu^{2+} ions are preferentially and rapidly adsorbed in the initial stage. With the further increase of contact time, the number of adsorption sites and OH^- groups are decreased, thus the adsorption rate is gradually decreased, finally reaching an equilibrium adsorption capacity in the subsequent process. The adsorption rates of Mn^{2+} and Ni^{2+} ions are relatively low in the initial

contact stage, because Cu^{2+} ions are preferentially adsorbed. When the adsorption of Cu^{2+} ions becomes saturated, the adsorption rates of Mn^{2+} and Ni^{2+} ions are gradually increased. The adsorption capacity of Mn^{2+} ions is higher than that of Ni^{2+} with the increase of time, which is mainly because the radius of Mn^{2+} is larger than that of Ni^{2+}.

Fig. 7(h) shows the XPS spectra of LDCC after adsorption of three heavy metal ions. It can be seen that the binding energy values at the peaks of Cu (Cu 2p3/2 and Cu 2p1/2 are at 934.4 eV and 954.3 eV) are higher than those of Mn (Mn 2p3/2 and Mn 2p1/2 are at 641.3 eV and 653.1 eV) and Ni (Ni 2p3/2 and Ni 2p1/2 are at 855.6 eV and 873.3 eV). As it is well-known, the higher the binding energy, the easier is for the substance to form chemical bonds. Therefore, in the co-existing system of Mn^{2+}, Cu^{2+} and Ni^{2+} ions, Cu^{2+} ions are easier to be adsorbed, if compared with those of Mn^{2+} and Ni^{2+} ions.

3.3 Discussions on adsorption mechanisms of LDCC

Adsorption kinetics is an important feature of the adsorption process, which is often studied from results of adsorption capacity (i.e., amount of adsorbate adsorbed by unit adsorbent) and contact time of the adsorption processes. To understand the adsorption mechanisms related to the adsorption process for the LDCC in this study, we have applied different kinetic models to compare with the experimentally obtained data. The following models are used in this study, e.g., pseudo-first-order, pseudo-second-order and intra-particle diffusion (IPD) kinetic models [61, 62], with their adsorption kinetics described by Eqs. (4)-(6), respectively:

$$ln\left(q_e\text{-}q_t\right) = \text{-}K_1 t + lnq_e \quad (4)$$

$$\frac{t}{q_t} = \frac{1}{K_2 q_e^2} + \frac{t}{q_e} \quad (5)$$

$$q_t = K_i t^{0.5} + C \quad (6)$$

where K_1, K_2 and K_i are pseudo-first-order, pseudo-second-order and intra-particle diffusion rate constants, respectively.

Fig. 8 shows the linear fitting results using the pseudo-first-order model, pseudo-second-order model and intra-particle diffusion model when the LDCC adsorbs the heavy metal ions. The fitting parameters used are presented in Table 1. Figs. 8(a)-(f)

show that for fitting the experimental data of LDCC adsorption of three heavy metal ions, the pseudo-second-order model shows a much higher correlation coefficient value (R^2). Compared with the pseudo-first-order model, the pseudo-second-order model shows a much better fitting result with a good linearity, and the theoretical adsorption capacity value is much closer to the experimental data of q_e. Therefore, we can conclude that the adsorbing process of the LDCC for heavy metal ions is dominated by the chemical adsorption process, which is consistent with those reported in the literature [55, 61]. Figs. 8(g)-(i) show the linear fitting results using the IPD model. It can be found that IPD model has produced two fitting stages [63]. The first fitting stage represents the diffusion of heavy metal ions on the surface of LDCC during the adsorption process. The second stage is a linear one, corresponding to the diffusion of heavy metal ions in the LDCC particles or pores. The curved section is mainly due to the boundary layer effect in the adsorption process of heavy metal ions. In addition, the R^2 value (<1) fitted by the IPD model does not pass through the origin, as shown in Figs. 8(g)-(i), indicating that IPD occurs in the adsorption process [64]. It shows that the adsorption process involves multiple steps, including quick adsorption at the outer surface and diffusion into the bulk material.

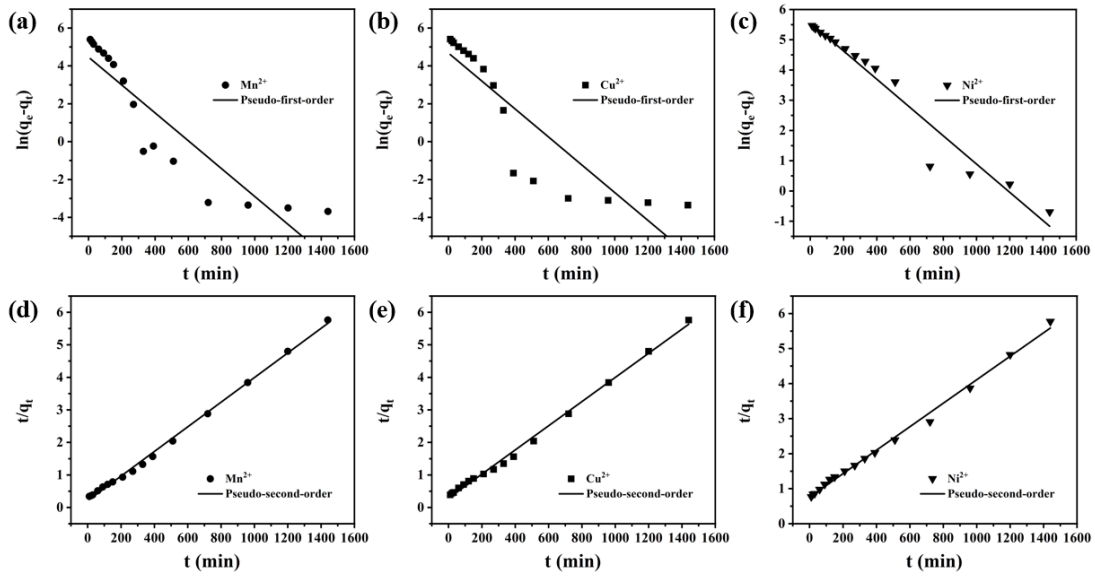

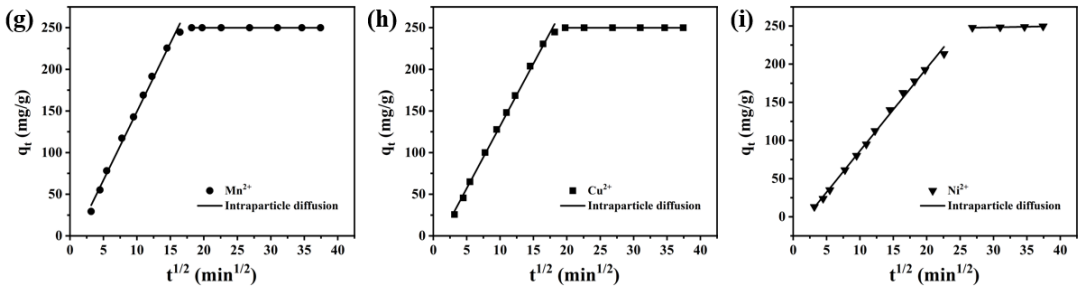

Fig. 8. (a) The fitting curves of the pseudo-first-order model. (b) The fitting curves of the pseudo-second-order model. (c) The fitting curves of the intra-particle diffusion model.

Table 1.

The kinetics parameters of the pseudo-first-order model, pseudo-second-order model and intra-particle diffusion model for Mn^{2+}, Cu^{2+} and Ni^{2+} adsorption on LDCC.

Heavy metal ions	Experimental	Pseudo-first-order model			Pseudo-second-order model			Intraparticle diffusion model			
	$q_{e,exp}$ (mg/g)	$q_{e,cal}$ (mg/g)	K_1 (min^{-1})	R^2	$q_{e,cal}$ (mg/g)	K_2 (g/mg·min)	R^2	K_{d1} (mg/g·min$^{0.5}$)	R_1^2	K_{d2} (mg/g·min$^{0.5}$)	R_2^2
Mn^{2+}	249.95	86.47	0.01695	0.8250	263.85	0.00007	0.9973	16.453	0.9934	0.00145	0.9259
Cu^{2+}	249.93	107.02	0.01902	0.9020	269.54	0.00005	0.9960	14.985	0.9964	0.00271	0.9946
Ni^{2+}	249.87	224.72	0.01075	0.9546	298.51	0.00001	0.9953	10.833	0.9961	0.15972	0.9458

Adsorption isotherms describes the relationship between the amount of adsorbate and the concentration of adsorbate at a constant temperature, which can be used to analyze and determine the maximum adsorption capacity of adsorbents. Langmuir isotherm model and Freundlich isotherm model were used to study the adsorption process in this study [60, 65]. These two adsorption isotherms models (i.e., Langmuir isotherm and Freundlich isotherm model) are expressed using the Eqs. (7) and (8):

$$\frac{C_e}{q_e} = \frac{1}{K_L q_m} + \frac{C_e}{q_m} \quad (7)$$

$$lnq_e = lnK_F + \frac{1}{n} lnC_e \quad (8)$$

where K_L is the Langmuir adsorption equilibrium constant (L/mg). K_F and n are the Freundlich constant and heterogeneity factor, respectively.

Fig. 9 shows the obtained adsorption isotherm curves of three heavy metal ions fitted using the Langmuir isotherm model and Freundlich isotherm model at different temperatures (e.g., 298 K, 308 K and 318 K). The corresponding fitting parameters are

listed in Table 2. Results show that compared with the Freundlich isotherm model, the Langmuir isotherm model shows a better linearity and a higher coefficient value, and its calculated q_e value is very close to the experimental value. These results show that the adsorption of Mn^{2+}, Cu^{2+} and Ni^{2+} ions by the LDCC is strongly linked to the monolayer chemical adsorption on the surface of adsorbent [58]. Results clearly show that the LDCC can be used to remove heavy metal ions due to its surface groups and unique micro- and nanostructures [66].

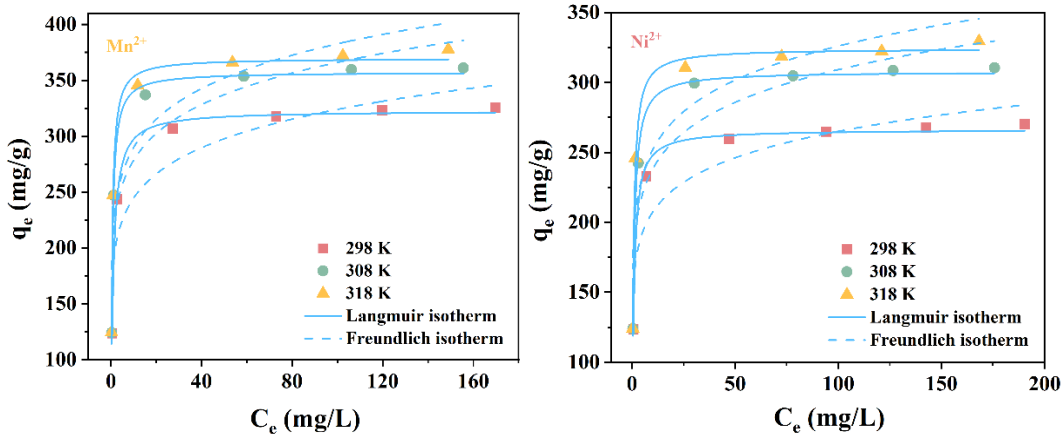

Fig. 9. Isothermal curves of LDCC adsorption of various heavy metals at different temperatures.

Table 2.

The kinetics parameters of the Langmuir model and Freundlich model for Mn^{2+}, Cu^{2+} and Ni^{2+} adsorption on LDCC.

Heavy metal ions	Langmuir model			Freundlich model		
	q_m	K_L	R^2	K_F	1/n	R^2
Mn^{2+}	325.60	0.47136	0.9980	156.234	0.16298	0.81847
Cu^{2+}	310.32	0.98014	0.9943	173.151	0.13306	0.80851
Ni^{2+}	268.95	0.60219	0.9977	144.329	0.13554	0.83194

Through the investigations of adsorption thermodynamics, the driving forces of the adsorption process and the influences of various factors on adsorption have been analyzed. The adsorption thermodynamics of Mn^{2+}, Cu^{2+} and Ni^{2+} ions onto the LDCC were studied at different temperatures (e.g., 298 K, 308 K and 318 K). The corresponding thermodynamic parameters including Gibbs free energy changes (ΔG^0), enthalpy changes (ΔH^0), and entropy changes (ΔS^0) at various temperatures of 298 K, 308 K and 318 K in the adsorption processes were calculated using Eqs. (9)-(11) [67]:

$$\Delta G^0 = -RT\ln K_C \quad (9)$$

$$\ln K_C = \frac{\Delta S^0}{R} - \frac{\Delta H^0}{RT} \quad (10)$$

$$K_C = \frac{q_e}{C_e} \quad (11)$$

where K_C is the Langmuir equilibrium constant at a given temperature. By plotting the relationships between $\ln K_C$ and 1000/T, the parameters ΔH^0 and ΔS^0 were calculated from the slope and intercept of the linear regression. The obtained results are summarized in Table 3. The calculated ΔG^0 values of Mn^{2+}, Cu^{2+} and Ni^{2+} ions are all negative, indicating that the adsorption processes of heavy metal ions onto LDCC were spontaneous processes [68]. Additionally, the values of ΔH^0 are greater than zero, which indicates that the adsorption is an endothermic process and confirms the results that the adsorption capacity of LDCC towards these heavy metal ions are increased with the increase of temperature [69]. The values of ΔS^0 are all larger than zero, indicating that there are increased solid/solution interfaces during the adsorption processes of Mn^{2+}, Cu^{2+} and Ni^{2+} ions [70].

Table 3. Thermodynamic parameters for the adsorption of Mn^{2+}, Cu^{2+} and Ni^{2+} ions on LDCC.

Heavy metal ions	T (K)	Thermodynamic parameters			
		$\ln K_C$	ΔG^0 (kJ/mol)	ΔS^0 (J/K·mol)	ΔH^0 (kJ/mol)
Mn^{2+}	298	0.651	-1.614	42.375	11.014
	308	0.841	-2.154		
	318	0.929	-2.456		
Ni^{2+}	298	0.350	-0.867	45.666	12.741
	308	0.569	-1.456		
	318	0.672	-1.777		

In order to explore the adsorption mechanism of LDCC for heavy metal ions, the surface compositions of LDCC samples before and after adsorption were further studied using the XPS. The binding states of heavy metal elements adsorbed on the surface of LDCC samples containing Mn^{2+}, Cu^{2+} and Ni^{2+} ions were further analyzed based on the high resolution spectra of various elements, and the results are shown in Figs. 10(a)-(c). In Fig. 10(a), The fitted Mn $2p_{3/2}$ peak at 641.3 eV shows that manganese was completely oxidized into a state of Mn^{4+}. This indicates that the main

adsorbate on the surface of LDCC sample is $MnO(OH)_2$, which is caused by the oxidation of $Mn(OH)_2$ in the air [67]. Fig. 10(b) shows that the characteristic peaks of Cu $2p_{3/2}$ and Cu $2p_{1/2}$ are at 934.4 eV and 954.3 eV, and two peaks at 942.5 eV and 962.1 eV are the satellite peaks of Cu $2p_{3/2}$ and Cu $2p_{1/2}$, respectively. The main fitted peaks of Cu $2p_{1/2}$ at 934.4 eV and Cu $2p_{1/2}$ at 954.3 eV are consistent with the binding energy values of $Cu(OH)_2$, which is also confirmed by the satellite peak at 942.5 eV [68]. This indicates that there is a layer of $Cu(OH)_2$ on the surface of LDCC, which is consistent with the color change of the sample after Cu^{2+} adsorption from the experimental observations. Similarly, as shown in Fig. 10(c), there are two peaks at binding energies of 861.7 eV and 879.5 eV, which are assigned to the satellite peaks of Ni $2p_{3/2}$ and Ni $2p_{1/2}$, respectively. The binding energy values of 855.6 eV and 873.3 eV are assigned to the characteristic peaks of Ni $2p_{3/2}$ and Ni $2p_{1/2}$, which can be confirmed by the presence of pale green $Ni(OH)_2$ on the surface of LDCC [69].

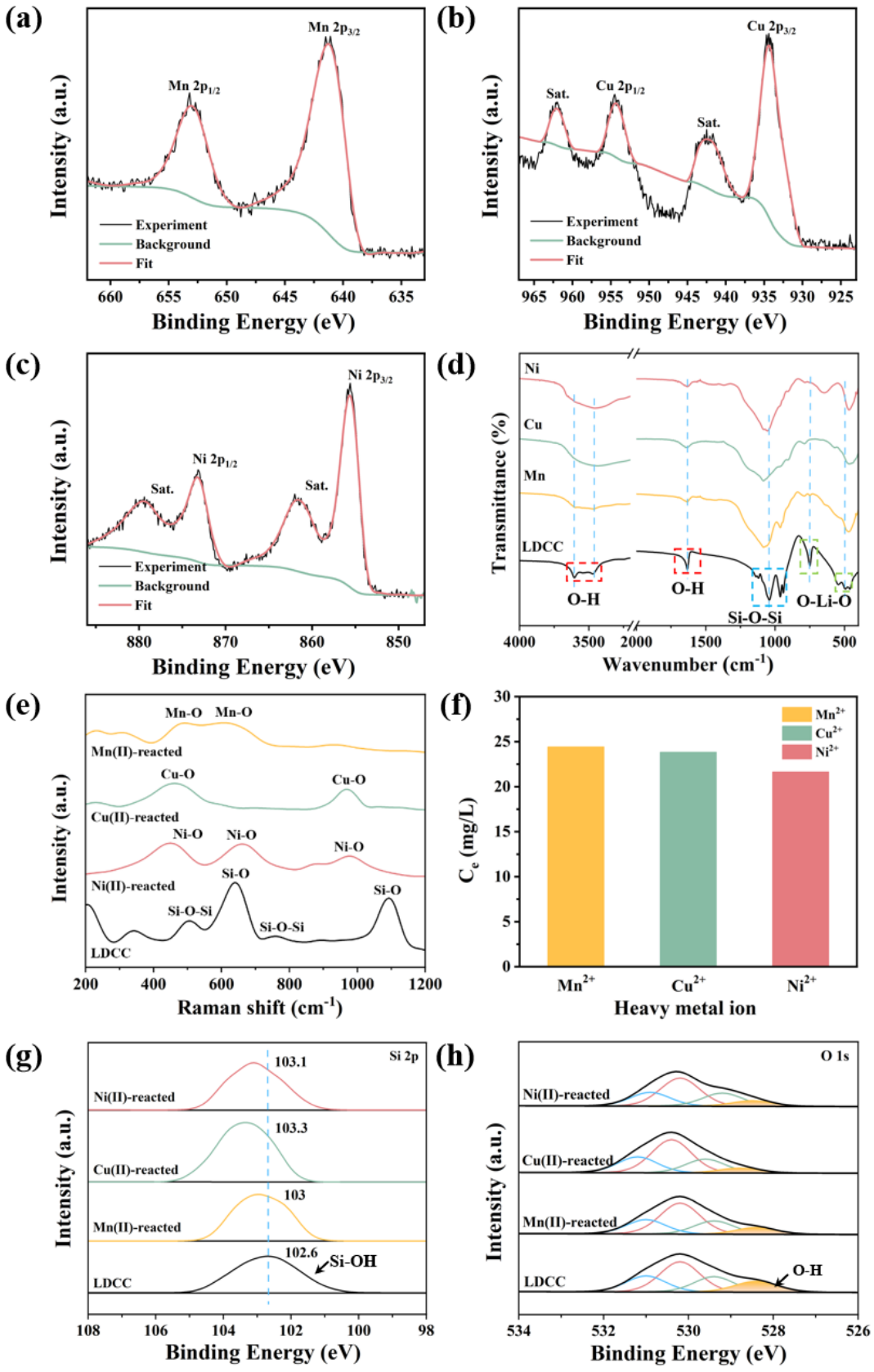

Fig. 10. (a-c) Mn 2p, Cu 2p and Ni 2p XPS spectra of LDCC after adsorption. (d) FT-IR spectra of LDCC before and after Mn^{2+}, Cu^{2+} and Ni^{2+} adsorption. (e) Raman spectra of LDCC before

and after Mn^{2+}, Cu^{2+} and Ni^{2+} adsorption. (f) Li^{+} concentration after LDCC adsorption. (g) Si 2p and (h) O 1s XPS spectra of LDCC after adsorption.

FTIR spectra of the LDCC before and after adsorption of heavy metal ions were obtained, and the results are shown in Fig. 10(d). The peak at 3603 cm^{-1} can be assigned to the stretching vibration mode of non-hydrogen-bonded hydroxyl (Si(OH)) in nanorod-like crystals, and the weak peak at 3477 cm^{-1} and the peak at 1637 cm^{-1} can be assigned to the vibrational mode of hydrogen-bonded hydroxyl groups [70]. After adsorption of heavy metal ions, the intensities of these three characteristic absorption peaks are decreased, indicating that OH^{-} groups on the surface of LDCC are reacted with heavy metal ions [71]. At the same time, the characteristic absorption peak of Si-O-Si at 1100 cm^{-1} due to asymmetric stretching has been shifted due to the electrostatic reactions between siloxane cage and metal ions [58]. The above analysis clearly reveals the interactions between hydroxyl and heavy metal ions in the adsorption process. In addition, the characteristic absorption peaks at 500 and 747cm^{-1} are attributed to the O-Li-O bending vibrations [72]. They are disappeared or shifted after absorption of heavy metal ions, indicating that Li^{+} interacts with heavy metal ions through an ion-exchange mechanism [73].

Fig. 10(e) shows the Raman spectrum of the composite before and after the adsorption of heavy metal ions. The characteristic peaks at 505 and 758 cm^{-1} are assigned to the bending vibrations of Si-O-Si bonds in Q^4 structural units, respectively. The peaks at 640 and 1093 cm^{-1} are assigned to the bending vibrations of Si-O in Q^3 structural units, respectively. After the composite completed the adsorption of heavy metals, the characteristic peaks of the composite were attenuated. At the same time, the Raman spectra of the adsorbed heavy metal ions also showed the characteristic peaks of heavy metals. The two broad peaks at 490 and 619 cm^{-1} are identified as the vibrations of the Mn-O stretching mode. The three broad peaks at 462 and 969 cm^{-1} are identified as the vibrations of the Cu-O stretching mode. The three broad peaks at 450, 664 and 980 cm^{-1} are identified as the vibrations of the Ni-O stretching mode.

Fig. 10(f) shows the equilibrium concentration of Li^{+} in the solution after the LDCC adsorbs three heavy metal ions with their initial concentration of 150 mg/L. It

can be seen that the concentration of Li^+ produced by the LDCC after adsorption of Mn^{2+}, Cu^{2+} and Ni^{2+} ions are 24.43, 23.83 and 21.65 mg/L, respectively. The concentration differences among these three ions are quite small, indicating that the Li^+ of LDCC is actively participated in the adsorption process through ion-exchange, but has a limited effect.

Fig. 10(g) shows the high-resolution XPS spectra of Si 2p after adsorption with heavy metal ions, which can be assigned to the Si-OH of LDCC at 102.6 eV. It was reported that after adsorption of heavy metal ions, these sites were transferred to a higher binding energy [55]. The O 1s spectra of LDCC before and after adsorption shown in Fig. 10(h) can be divided into four different peaks. Compared with the O 1s spectra of LDCC before adsorption, the peak area ratio corresponding to hydroxyl in the O 1s spectra after adsorption is significantly reduced. It clearly shows that the hydroxyl groups in the LDCC are involved in the adsorption process [53]. The significant peak shifts of Si 2p and O 1s indicate the strong adsorption of heavy metal ions of oxygen-containing functional groups. These reactions can be described using Eqs. (12)-(15):

$$Mn^{2+} + 2OH^- \rightarrow Mn(OH)_2 \quad (12)$$

$$2Mn(OH)_2 + O_2 \rightarrow 2MnO(OH)_2 \quad (13)$$

$$Cu^{2+} + 2OH^- \rightarrow Cu(OH)_2 \quad (14)$$

$$Ni^{2+} + 2OH^- \rightarrow Ni(OH)_2 \quad (15)$$

In addition, the surface areas and pore structures of LDCC before and after the adsorption of heavy metal ions were characterized by the N_2 adsorption-desorption method. The results are shown in Fig. 11 and Table 4. The type IV curve of the composite shown in Fig. 4(c) and that of LDCC after the adsorption are similar. The specific surface area and pore volume of the composite are increased after cycling. The reason may be that some products were formed by complexation, such as $Ni(OH)_2$, and they were remained in the composite after several cycling. The accumulation of these complexes on the surface of the composite produced accumulation pores, which led to the increases of specific surface area and pore volume [74], which confirms that the adsorption of heavy metal ions by the composite is a chemical adsorption.

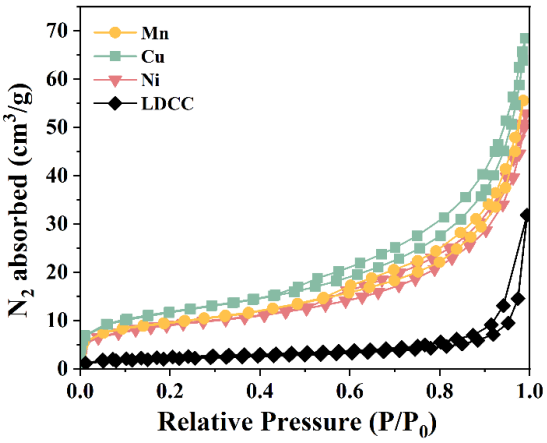

Fig. 11. N_2 adsorption-desorption isotherms of the LDCC before and after cycling.

Table 4.

Textural characteristics of the LDCC before and after cycling.

Samlple	S_{BET} (m^2/g)	Total Pore Volume (cm^3/g)	Average Pore Size (nm)
LDCC after Mn^{2+}	35.1543	0.08916	9.7617
LDCC after Cu^{2+}	41.7838	0.10583	10.1308
LDCC after Ni^{2+}	32.9167	0.07775	9.2164
LDCC	9.2709	0.01481	8.1467

Fig. 12 shows the surface morphology and EDX results of the LDCC after its adsorption of Mn^{2+}, Cu^{2+} and Ni^{2+} ions. It can be seen that except for Si and O elements of the LDCC, Mn, Cu and Ni elements are all evenly distributed on the surface of LDCC, indicating that the adsorption is relatively uniform. Figs. 12(a), (b) and (c) show clearly the brown loaded products after Mn^{2+} adsorption, the blue loaded products after Cu^{2+} adsorption, and the light green loaded products after Ni^{2+} adsorption, respectively. This is dramatically different with the white loaded products on the original substrate (carbon cloth) surface (Fig. 2). This significant color changes clearly show that LDCC nanorods can be effectively used for heavy metal adsorbents, which is consistent with XPS analysis results. As shown in Fig. 3, the adsorbed nanorod structures are strongly adhered onto carbon cloth and form evenly distributed clusters of nanorods. There are also some irregularly flower-like clusters attachments which are identified as the adsorbed heavy metal ions. It is worthwhile to note that the

morphology of nanorods have hardly been modified, revealing their very stable structures.

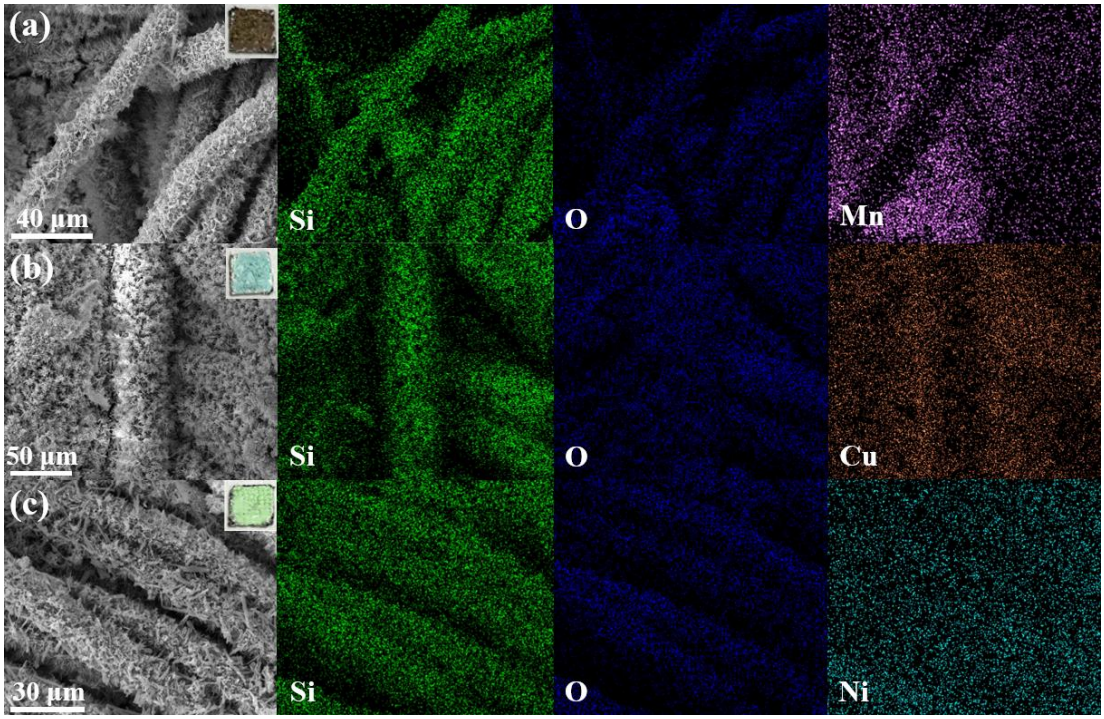

Fig. 12. SEM and EDX images of LDCC after adsorption: (a) Mn^{2+}, (b) Cu^{2+}, (c) Ni^{2+}. The insets are the color change of LDCC after adsorption.

Based on the above analysis, we proposed adsorption mechanisms of the LDCC for the heavy metal ions, which are illustrated shown in Fig. 13. Firstly, due to the strong interactions between liquid and the hydroxyl groups of LDCC, heavy metal ions are adsorbed onto the LDCC. Secondly, on the surfaces of LDCC, heavy metal ions and LDCC have ion-exchange reactions (mainly through lithium ions). In addition, the nanobrush-like structures of nanorods on the carbon cloth are advantageous for the adsorption of heavy metal ions, providing numerous active sites and enhancing ions' diffusions, thus promoting the adsorption and resulting in an excellent adsorption performance through the synergistic effects.

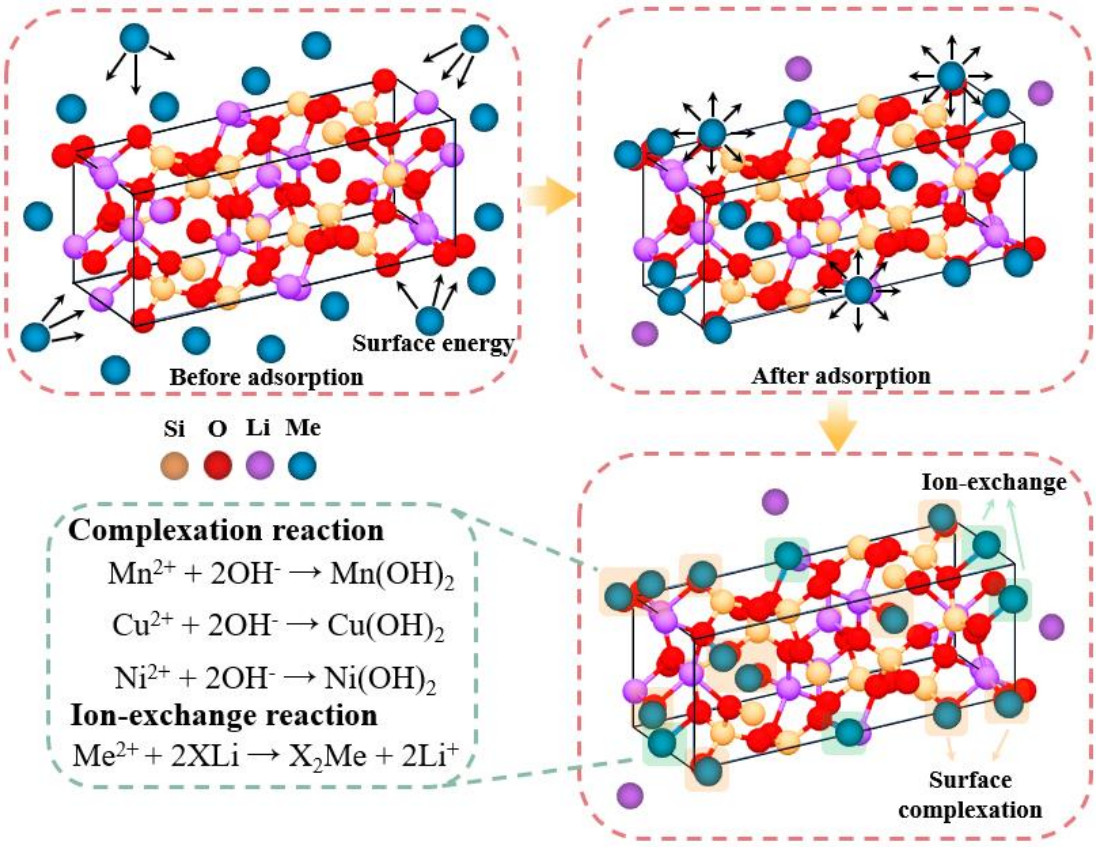

Fig. 13. The adsorption mechanism of Mn^{2+}, Cu^{2+} and Ni^{2+} by LDCC.

4. Conclusion

In this paper, nanobrush-like $Li_2Si_2O_5$ composites (LDCC) and uniform microstructures have been successfully prepared using the lithium hydroxide and tetraethyl orthosilicate as raw materials, deposited onto the carbon cloth used as the supporting materials. The composites were synthesized using a hydrothermal method at 180℃ for 6 hrs with a Li/Si ratio of 1:1. The adsorption behavior of LDCC for heavy metal ions was explained using the pseudo-second-order model and Langmuir isothermal model, indicating that the adsorption process was the monolayer chemical adsorption. The maximum adsorption capacities of Mn^{2+}, Cu^{2+}, Ni^{2+} ions were 325.60, 312.12 and 270.15 mg/g at 298 K, respectively. In addition, the LDCC had a preferred adsorption for Cu^{2+} ions. The unique nanobrush-like structure with its numerous surface groups and active sites significantly enhanced the adsorption of heavy metal ions. The adsorption mechanisms are mainly attributed to the surface interactions

between heavy metal ions and hydroxyl groups, along with the ion-exchange between a small amount of heavy metal ions and lithium ions.

Acknowledgments

The authors would like to acknowledge the financial supports from the Science and Technology Project of Shaanxi Province of China (No.2020ZDLGY12-06), Xi'an Science research project of China (No.2021XJZZ0042) and International Exchange Grant (IEC/NSFC/201078) through Royal Society and National Science Foundation of China (NSFC).

References

[1] F. Lu, D. Astruc, Nanocatalysts and other nanomaterials for water remediation from organic pollutants, Coordination Chemistry Reviews 408 (2020) 213180.

[2] W.T. Tan, H. Zhou, S.F. Tang, P. Zeng, J.F. Gu, B.H. Liao, Enhancing Cd(II) adsorption on rice straw biochar by modification of iron and manganese oxides, Environ Pollut 300 (2022) 118899.

[3] Y.-Y. Yu, Q.-W. Cheng, C. Sha, Y.-X. Chen, S. Naraginti, Y.-C. Yong, Size-controlled biosynthesis of FeS nanoparticles for efficient removal of aqueous Cr(VI), Chemical Engineering Journal 379 (2020) 122404.

[4] C. Xu, Y. Feng, H. Li, R. Wu, J. Ju, S. Liu, Y. Yang, B. Wang, Adsorption of heavy metal ions by iron tailings: Behavior, mechanism, evaluation and new perspectives, Journal of Cleaner Production 344 (2022) 131065.

[5] L.S. Miranda, G.A. Ayoko, P. Egodawatta, A. Goonetilleke, Adsorption-desorption behavior of heavy metals in aquatic environments: Influence of sediment, water and metal ionic properties, J Hazard Mater 421 (2022) 126743.

[6] H. Yue, Z. Shang, P. Xu, D. Feng, X. Li, Preparation of EDTA modified chitooligosaccharide/sodium alginate/Ca2+ physical double network hydrogel by using of high-salinity oilfield produced water for adsorption of Zn2+, Ni2+ and Mn2+, Separation and Purification Technology 280 (2022) 119767.

[7] H. Ye, C. Liu, M.-B. Wu, L.-L. Ma, S.-C. Liu, Y. Zhong, J. Yao, Amyloid-like assembly converting commercial proteins to water-insoluble adsorbents with ultrahigh adsorption capacity and excellent antifouling property for uranium extraction, Journal of Materials Chemistry A 10 (2022) 2987.
[8] C. Wu, J. Gao, Y. Liu, W. Jiao, G. Su, R. Zheng, H. Zhong, High-gravity intensified electrodeposition for efficient removal of Cd2+ from heavy metal wastewater, Separation and Purification Technology 289 (2022) 120809.
[9] J. Liu, Q. Liu, J. Li, X. Zheng, Z. Liu, X. Guan, Photochemical conversion of oxalic acid on heterojunction engineered FeWO4/g-C3N4 photocatalyst for high-efficient synchronous removal of organic and heavy metal pollutants, Journal of Cleaner Production 363 (2022) 123527.
[10] E. Ragheb, M. Shamsipur, F. Jalali, F. Mousavi, Modified magnetic-metal organic framework as a green and efficient adsorbent for removal of heavy metals, Journal of Environmental Chemical Engineering 10 (2022) 107297.
[11] W. Gong, K. Zheng, C. Zhang, L. Liu, Y. Shan, J. Yao, Simultaneous and efficient removal of heavy metal ions and organophosphorus by amino-functionalized cellulose from complex aqueous media, Journal of Cleaner Production 367 (2022) 133040.
[12] Z. Ren, L. Wang, Y. Li, J. Zha, G. Tian, F. Wang, H. Zhang, J. Liang, Synthesis of zeolites by in-situ conversion of geopolymers and their performance of heavy metal ion removal in wastewater: A review, Journal of Cleaner Production 349 (2022) 131441.
[13] H.J. Hong, J.S. Lim, J.Y. Hwang, M. Kim, H.S. Jeong, M.S. Park, Carboxymethlyated cellulose nanofibrils (CMCNFs) embedded in polyurethane foam as a modular adsorbent of heavy metal ions, Carbohydr Polym 195 (2018) 136.
[14] D. Zhang, J. Li, J. Liang, H. Li, Y. Yan, Self-assembly of α-MoO3 flower as a highly effective organics adsorbent for water purification, Journal of the American Ceramic Society 102 (2018) 3307.
[15] L. Shen, W. Ding, X. Li, Y. Zhang, Y. Cong, Fabrication of 3D self-supported MoS2-Co-P/nickel foam electrode for adsorption-electrochemical removal of Cr(IV), Chemosphere 304 (2022) 135209.

[16] C. Gao, H. Wang, T. Yu, Y. Li, L. Liu, Self-sustained recovery of silver with stainless-steel based Cobalt/Molybdenum/Manganese polycrystalline catalytic electrode in bio-electroreduction microbial fuel cell (BEMFC), J Hazard Mater 424 (2022) 127664.
[17] R. Zheng, Q. Lin, L. Meng, C. Zhang, L. Zhao, M. Fu, J. Ren, Flexible phosphorus-doped activated carbon fiber paper in-situ loading of CuO for degradation of phenol, Separation and Purification Technology 298 (2022) 121619.
[18] R. Jia, Q. Tao, D. Sun, Y. Dang, Carbon cloth self-forming dynamic membrane enhances anaerobic removal of organic matter from incineration leachate via direct interspecies electron transfer, Chemical Engineering Journal 445 (2022) 136732.
[19] H. Tahzibi, S. Azizian, Fabrication of superhydrophobic-icephobic carbon cloth using polydimethylsiloxane for oil–water separation, Journal of Molecular Liquids 356 (2022) 119008.
[20] M. Shamsayei, Y. Yamini, H. Asiabi, M.M. Khataei, Electrodeposition of layered double hydroxide intercalated with 2,3-dimercaptopropane sulfonate on carbon cloth and application for effective uptake of heavy metals, Applied Clay Science 196 (2020) 105747.
[21] E. Mosayebi, S. Azizian, Study of copper ion adsorption from aqueous solution with different nanostructured and microstructured zinc oxides and zinc hydroxide loaded on activated carbon cloth, Journal of Molecular Liquids 214 (2016) 384.
[22] X. Liu, J. Wang, Electro-assisted adsorption of Cs(I) and Co(II) from aqueous solution by capacitive deionization with activated carbon cloth/graphene oxide composite electrode, Sci Total Environ 749 (2020) 141524.
[23] X. Wang, J. Wang, W. Teng, Y. Du, J. Wu, F. Guo, B. Chen, Fabrication of highly efficient magnesium silicate and its adsorption behavior towards Cr(VI), Microporous and Mesoporous Materials 323 (2021) 111196.
[24] Z. Jia, C. Han, L. Wu, D. Zhang, M. Li, Biotemplated synthesis of hollow nickel silicate fiber for organic dye contaminants and its selective adsorption, Colloids and Surfaces A: Physicochemical and Engineering Aspects 648 (2022) 129219.

[25] F. Valenzuela, G. Quintana, A. Briso, V. Ide, C. Basualto, J. Gaete, G. Montes, Cu(II), Cd(II), Pb(II) and As(V) adsorption from aqueous solutions using magnetic iron-modified calcium silicate hydrate: Adsorption kinetic analysis, Journal of Water Process Engineering 40 (2021) 101951.

[26] Z. Sun, Y. Liu, C. Srinivasakannan, One-pot fabrication of rod-like magnesium silicate and its adsorption for Cd2+, Journal of Environmental Chemical Engineering 8 (2020) 104380.

[27] S. Bai, G. Tian, L. Gong, Q. Tang, J. Meng, X. Duan, J. Liang, Mesoporous manganese silicate composite adsorbents synthesized from high-silicon iron ore tailing, Chemical Engineering Research and Design 159 (2020) 543.

[28] H. Zhang, Z. He, Y. Zhang, W. Jing, B. Wang, J. Yang, I. Lloyd, Lithium Disilicate Glass-Ceramics by Heat Treatment of Lithium Metasilicate Glass-Ceramics Obtained by Hot Pressing, Journal of the American Ceramic Society 98 (2015) 3659.

[29] H. Zhang, B. Sun, Y. Qian, T. Yang, W. Chen, CTAB-mediated lithium disilicate branched structures as superb adsorbents to remove Mn2+ in water, Boletín de la Sociedad Española de Cerámica y Vidrio (2022).

[30] C.X. Gui, Q.Q. Wang, S.M. Hao, J. Qu, P.P. Huang, C.Y. Cao, W.G. Song, Z.Z. Yu, Sandwichlike magnesium silicate/reduced graphene oxide nanocomposite for enhanced Pb2+ and methylene blue adsorption, ACS Appl Mater Interfaces 6 (2014) 14653.

[31] H. Zhang, J. Yang, Hollow Li2SiO3 architectures with tunable secondary nanostructures and their potential application for the removal of heavy metal ions, Journal of Materials Science 55 (2019) 3845.

[32] H. Zhang, J. Wang, J. Yang, Hydrothermal synthesis and methylene blue adsorption performance of novel 3D hierarchical Li2Si2O5 hydrate particles, Sci Rep 10 (2020) 5545.

[33] K. Sangwal, Growth kinetics and surface morphology of crystals grown from solutions Recent observations and their interpretations, Prog. Energy Combust. Sci 36 (1998) 163.

[34] K. Sato, A. Tamai, K. Ohara, H. Kiuchi, E. Matsubara, Non-destructive observation of plated lithium distribution in a large-scale automobile Li-ion battery using synchrotron X-ray diffraction, Journal of Power Sources 535 (2022) 231399.
[35] H. Zhang, J. Wang, J. Yang, Anisotropic growth and photoluminescence of Li2Si2O5 hydrate rods, Journal of Materials Science: Materials in Electronics 30 (2019) 17405.
[36] J. Liu, Z.-Y. Hu, Y. Peng, H.-W. Huang, Y. Li, M. Wu, X.-X. Ke, G.V. Tendeloo, B.-L. Su, 2D ZnO mesoporous single-crystal nanosheets with exposed {0001} polar facets for the depollution of cationic dye molecules by highly selective adsorption and photocatalytic decomposition, Applied Catalysis B: Environmental 181 (2016) 138-145.
[37] M. Kim, D. Park, J. Kim, A thermoelectric generator comprising selenium-doped bismuth telluride on flexible carbon cloth with n-type thermoelectric properties, Ceramics International 48 (2022) 10852.
[38] M. Kruk, M. Jaroniec, Gas Adsorption characterization of ordered organic inorganic nanocomposite materials, Chem, Mater.,13 (2001) 3169.
[39] Y. Yuan, Z. An, R. Zhang, X. Wei, B. Lai, Efficiencies and mechanisms of heavy metals adsorption on waste leather-derived high-nitrogen activated carbon, Journal of Cleaner Production 293 (2021) 126215.
[40] V. Vit, F. Orlandi, A. Griesi, D. Bersani, D. Calestani, F. Cugini, M. Solzi, M. Gemmi, L. Righi, Mechanosynthesis of multiferroic hybrid organic-inorganic [NH4][M(HCOO)3]M = Co2+,Mn2+,Zn2+,Ni2+,Cu2+ formate-based frameworks, Journal of Alloys and Compounds 899 (2022) 163288.
[41] S. Tang, J. Yang, L. Lin, K. Peng, Y. Chen, S. Jin, W. Yao, Construction of physically crosslinked chitosan/sodium alginate/calcium ion double-network hydrogel and its application to heavy metal ions removal, Chemical Engineering Journal 393 (2020) 124728.
[42] R. Xu, G. Zhou, Y. Tang, L. Chu, C. Liu, Z. Zeng, S. Luo, New double network hydrogel adsorbent: Highly efficient removal of Cd(II) and Mn(II) ions in aqueous solution, Chemical Engineering Journal 275 (2015) 179.

[43] Y. Xue, W. Cheng, M. Cao, J. Gao, J. Chen, Y. Gui, W. Zhu, F. Ma, Development of nitric acid-modified activated carbon electrode for removal of Co(2+)/Mn(2+)/Ni(2+) by electrosorption, Environ Sci Pollut Res Int (2022).
[44] Y. Zhou, X. Wang, J. Men, M. Jia, C. Liang, Study on the adsorption performance of zeolitic imidazolate framework-8 (ZIF-8) for Co2+ and Mn2+, Journal of Radioanalytical and Nuclear Chemistry 331 (2022) 1367.
[45] Q. An, Y. Miao, B. Zhao, Z. Li, S. Zhu, An alkali modified biochar for enhancing Mn2+ adsorption: Performance and chemical mechanism, Materials Chemistry and Physics 248 (2020) 122895.
[46] E.C. Peres, D. Pinto, M.S. Netto, E.S. Mallmann, L.F.O. Silva, E.L. Foletto, G.L. Dotto, Adsorption kinetics and equilibrium of Ni(2+), Cu(2+), Co(2+), and Ag(+) on geopolymers derived from ashes: application to treat effluents from the E-Coat printing process, Environ Sci Pollut Res Int 29 (2022) 70158.
[47] M.I. Shariful, T. Sepehr, M. Mehrali, B.C. Ang, M.A. Amalina, Adsorption capability of heavy metals by chitosan/poly(ethylene oxide)/activated carbon electrospun nanofibrous membrane, Journal of Applied Polymer Science 135 (2018) 45851.
[48] J. Xiao, R. Hu, G. Chen, B. Xing, Facile synthesis of multifunctional bone biochar composites decorated with Fe/Mn oxide micro-nanoparticles: Physicochemical properties, heavy metals sorption behavior and mechanism, J Hazard Mater 399 (2020) 123067.
[49] Z. Yin, L. Zhu, F. Mo, S. Li, D. Hu, R. Chu, C. Liu, C. Hu, Preparation of biochar grafted with amino-riched dendrimer by carbonization, magnetization and functional modification for enhanced copper removal, Journal of the Taiwan Institute of Chemical Engineers 121 (2021) 349.
[50] R. Zare-Dorabei, S.M. Ferdowsi, A. Barzin, A. Tadjarodi, Highly efficient simultaneous ultrasonic-assisted adsorption of Pb(II), Cd(II), Ni(II) and Cu(II) ions from aqueous solutions by graphene oxide modified with 2,2'-dipyridylamine: Central composite design optimization, Ultrason Sonochem 32 (2016) 265.

[51] S. Biswas, B.C. Meikap, T.K. Sen, Adsorptive Removal of Aqueous Phase Copper (Cu2+) and Nickel (Ni2+) Metal Ions by Synthesized Biochar–Biopolymeric Hybrid Adsorbents and Process Optimization by Response Surface Methodology (RSM), Water, Air, & Soil Pollution 230 (2019) 197.
[52] M.A. Djilali, H. Mekatel, M. Mellal, M. Trari, Synthesis and characterization of MgCo2O4 nanoparticles: Application to removal of Ni2+ in aqueous solution by adsorption, Journal of Alloys and Compounds 907 (2022) 164498.
[53] Z. Wu, W. Deng, W. Zhou, J. Luo, Novel magnetic polysaccharide/graphene oxide @Fe3O4 gel beads for adsorbing heavy metal ions, Carbohydr Polym 216 (2019) 119.
[54] F. Arshad, M. Selvaraj, J. Zain, F. Banat, M.A. Haija, Polyethylenimine modified graphene oxide hydrogel composite as an efficient adsorbent for heavy metal ions, Separation and Purification Technology 209 (2019) 870.
[55] W. Wang, Z. Chen, H. Zhou, Y. Zhang, X. Wang, Two-dimensional lamellar magnesium silicate with large spacing as an excellent adsorbent for uranium immobilization, Environmental Science: Nano 5 (2018) 2406.
[56] J.B. Neris, F.H.M. Luzardo, E.G.P. da Silva, F.G. Velasco, Evaluation of adsorption processes of metal ions in multi-element aqueous systems by lignocellulosic adsorbents applying different isotherms: A critical review, Chemical Engineering Journal 357 (2019) 404.
[57] F. Yuan, C. Wu, Y. Cai, L. Zhang, J. Wang, L. Chen, X. Wang, S. Yang, S. Wang, Synthesis of phytic acid-decorated titanate nanotubes for high efficient and high selective removal of U(VI), Chemical Engineering Journal 322 (2017) 353.
[58] W. Zhou, P. Wu, L. Zhang, D. Zhu, X. Zhao, Y. Cai, Heavy metal ions and particulate pollutants can be effectively removed by a gravity-driven ceramic foam filter optimized by carbon nanotube implantation, J Hazard Mater 421 (2022) 126721.
[59] Y. Elakneswaran, T. Nawa, K. Kurumisawa, Electrokinetic potential of hydrated cement in relation to adsorption of chlorides, Cement and Concrete Research 39 (2009) 340.

[60] S. Cho, J.-H. Kim, K.S. Yang, M. Chang, Facile preparation of amino-functionalized polymeric microcapsules as efficient adsorbent for heavy metal ions removal, Chemical Engineering Journal 425 (2021) 130645.
[61] D. Jiang, Y. Yang, C. Huang, M. Huang, J. Chen, T. Rao, X. Ran, Removal of the heavy metal ion nickel (II) via an adsorption method using flower globular magnesium hydroxide, J Hazard Mater 373 (2019) 131.
[62] L. Kong, Y. Ruan, Q. Zheng, M. Su, Z. Diao, D. Chen, L. Hou, X. Chang, K. Shih, Uranium extraction using hydroxyapatite recovered from phosphorus containing wastewater, J Hazard Mater 382 (2020) 120784.
[63] R. Wang, L. Deng, X. Fan, K. Li, H. Lu, W. Li, Removal of heavy metal ion cobalt (II) from wastewater via adsorption method using microcrystalline cellulose-magnesium hydroxide, Int J Biol Macromol 189 (2021) 607.
[64] E. Orozco-Guareno, F. Santiago-Gutierrez, J.L. Moran-Quiroz, S.L. Hernandez-Olmos, V. Soto, W. de la Cruz, R. Manriquez, S. Gomez-Salazar, Removal of Cu(II) ions from aqueous streams using poly(acrylic acid-co-acrylamide) hydrogels, J Colloid Interface Sci 349 (2010) 583.
[65] M.A. Al-Ghouti, D.A. Da'ana, Guidelines for the use and interpretation of adsorption isotherm models: A review, J Hazard Mater 393 (2020) 122383.
[66] S.-M. Hao, J. Qu, Z.-S. Zhu, X.-Y. Zhang, Q.-Q. Wang, Z.-Z. Yu, Hollow Manganese Silicate Nanotubes with Tunable Secondary Nanostructures as Excellent Fenton-Type Catalysts for Dye Decomposition at Ambient Temperature, Advanced Functional Materials 26 (2016) 7334.
[67] G. Lv, F. Bin, C. Song, K. Wang, J. Song, Promoting effect of zirconium doping on Mn/ZSM-5 for the selective catalytic reduction of NO with NH 3, Fuel 107 (2013) 217.
[68] D. Hwan Kim, D. Hwa Kwak, H. Jun Tak, Y. Jung, K. Jung, S.-H. Park, J. Soo Ko, Room temperature synthesis of highly transparent CuO and Cu(OH)2 nanowire films via a simple wet chemical method, Applied Surface Science 590 (2022) 153083.

[69] G. Liu, Y. Qin, Y. Lyu, M. Chen, P. Qi, Y. Lu, Z. Sheng, Y. Tang, Low-crystalline β-Ni(OH)2 nanosheets on nickel foam with enhanced areal capacitance for supercapacitor applications, Chemical Engineering Journal 426 (2021) 131248.
[70] Q. Ge, H. Liu, Tunable amine-functionalized silsesquioxane-based hybrid networks for efficient removal of heavy metal ions and selective adsorption of anionic dyes, Chemical Engineering Journal 428 (2022) 131370.
[71] G. Zhao, J. Li, X. Ren, C. Chen, X. Wang, Few-layered graphene oxide nanosheets as superior sorbents for heavy metal ion pollution management, Environ Sci Technol 45 (2011) 10454.
[72] S. Nair, R. Raghavan, A kinetic study of CO2 sorption/desorption of lithium silicate synthesized through a ball milling method, Thermochimica Acta 699 (2021) 178918.
[73] N. Supriya, R. Rajeev, Synthesis and characterization of lithium silicates from organosilicone precursors for carbon dioxide adsorption, Journal of Thermal Analysis and Calorimetry 147 (2020) 135.